Self-consistent numerical-basis-set linear-combination-of-atomic-orbitals investigation of the electronic structure and properties of TiS_2†

Alex Zunger
Physics Department and Materials Research Center, Northwestern University, Evanston, Illinois 60201

A. J. Freeman
Physics Department and Materials Research Center, Northwestern University, Evanston, Illinois 60201 and Argonne National Laboratory, Argonne, Illinois 60439

(Received 28 January 1977)

A fully-self-consistent numerical-basis-set linear-combination-of-atomic-orbitals calculation of the electronic structure of TiS_2 is reported using the method described previously. The calculated band structure differs considerably from those previously obtained by non-self-consistent muffin-tin models. Comparison with experiment shows that the calculated optical properties for energies below 16 eV and the various characteristics of the valence and conduction bands agree very well with optical-absorption and electron-energy-loss data as well as with photoemission, x-ray absorption, and appearance-potential spectra. A small indirect gap (0.2–0.3 eV) occurs at the points M and L in the Brillouin zone with a larger direct gap (0.8 eV) at Γ. We suggest that the characteristic semi-metallic large g value observed experimentally originates from a near coincidence of the band gap with the enhanced spin-orbit splitting which is consistent with the soft-x-ray data and our band model. The bonding mechanism in TiS_2 is discussed in detail; it is shown by a direct calculation of the self-consistent charge density and the transverse effective charge that the system is predominantly covalent with small static ionic character and large dynamic ionicity. In contrast with muffin-tin $X\alpha$ models, the bonding is found to be largely due to Ti $4s4p$ to S $3p$ bonds and a much weaker Ti $3d$ to S $3p$ bond. The effects of muffin-tin approximation and self-consistency are discussed in detail. Extrapolation of these results to the case of $TiSe_2$ is made and the possible origin of its charge-density wave is discussed.

I. INTRODUCTION

The renewed experimental and theoretical interest in the layered transition-metal dichalcogenides has brought about in the last few years much greater understanding of their unusual anisotropic optical and transport properties,[1] and, more recently, those properties associated with the observation of charge-density waves[2] in some of these systems. Perhaps an outstanding exception is $1T$-TiS_2 for which the available information is still in a state of flux and conflict. For example, while optical experiments[3] have suggested that TiS_2 is a semiconductor with a gap of about 1–2 eV, recent temperature-dependent resistivity measurements on high-purity stoichiometric samples[4,5] demonstrated a semimetallic behavior and a remarkable temperature-dependent electrical resistivity proportional to T^2 from at least 10–400 K. Similarly, the theoretical description has had its difficulties. An early non-self-consistent Korringa-Kohn-Rostoker (KKR) calculation in the muffin-tin (MT) approximation[6] showed a fundamental gap of 2.0 eV at Γ and a smaller indirect gap of 1.4 eV between Γ and L. Further, while some of the calculated interband transition energies in the MT-KKR model could be reconciled with the observed data only after a rigid shift of about 1.4 eV was introduced in the theoretical transition energies, an empirical non-self-consistent tight-binding model[7,8] with parameters chosen to fit these observed optical transitions yields (a) a valence-band width about a factor of 2 too small (relative to the x-ray photoemission data[9–11]) and (b) a similar underestimation of the d-conduction-band width (compared with the observed appearance-potential spectra[12]). Similar contradictions occur in the various one-electron models derived to explain absorption mechanisms in TiS_2: while the semiempirical (optical data) model of Murray *et al.*[7] suggests the occurrence of a nonoverlapping metal d band in the gap formed between the bonding and antibonding metal-nonmetal s-p bands (σ-σ^* gap), the crystal-field model of Husiman *et al.*,[13] suggests that the metal d band appears in the valence-band continuum. By contrast, x-ray photoemission of Williams and Shepherd[10] places the lower part of the d band in partial overlap with the valence band, while a second component of this band appears in the antibonding σ^* region.

In this paper, we present the results of an *ab initio* theoretical study of the electronic properties of TiS_2 using our self-consistent numerical-basis-set linear-combination-of-atomic-orbitals (LCAO) method.[14,15] This method uses an accurate nonlinearly optimized (exact) atomic basis set for all core, valence, and some virtual states of the atoms appearing in the unit cell. All interaction and overlap integrals are evaluated accurately using a three-dimensional numerical Diophantine integra-

tion method.[15,16] Full self-consistency is obtained in a scheme that does not restrict the form of the crystalline charge density to any particular shape (viz., cellular or MT schemes[17] that spherically average the charge density around each site before the next iteration is attempted or iterative LCAO schemes that represent the charge density as a lattice sum of spherically symmetric atomic densities[18]). All non-MT contributions to the potential are fully retained and the electron local-density correlation functional[19,20] is treated as an intrinsic part of the crystal potential. The resulting self-consistent band structure indicates that stoichiometric TiS_2 is a semiconductor with a very small indirect band gap (of the order of 0.2–0.3 eV) separating the unoccupied d-based bands from the valence σ bands. The bonding mechanism is predominantly covalent with some minor ionic character and involves a metal s, p to nonmetal s, p chemical bond. The major metal atom configuration in the solid is the split-valence Ti $3d^{2-x}4s^{2-y}4p^{z}$ configuration with $x \cong 0.02e$, $y = 0.8e$, and $z \cong 0.4e$ (compared with the values of $x=y=z=0$ in the free-atom limit) in which substantial intra-atomic $4s$ to $4p$ electron promotion takes place, along with an interatomic charge redistribution that results in an increased population of the sulphur $3p$ shell.

II. THEORETICAL FORMULATION AND DESCRIPTION OF THE METHOD

Since a detailed description of our method of calculation was given elsewhere,[14,15] we outline here only those features which are pertinent for understanding the TiS_2 investigation. In this study we solve self-consistently (SC) the one-particle local-density equations, in which the crystal effective potential[19–22] includes the usual $\alpha\rho^{1/3}(\vec{r})$ (with $\alpha = \frac{2}{3}$) in the exchange potential $V_{ex}(\vec{r})$ and the free-electron correlation potential $V_{corr}(\vec{r})$ given by Singwi *et al.*[20] as fitted to an analytic form by Hedin and Lundqvist,[22] both obtained from the total ground-state electronic charge density

$$\rho_{cry}(\vec{r}) = \frac{N\Omega}{(2\pi)^3} \sum_{j=1}^{\sigma_{oc}} \int_{BZ} n_j(\vec{k}) \psi_j^*(\vec{k},\vec{r}) \psi_j(\vec{k},\vec{r})\, d\vec{k} \ . \quad (1)$$

In addition, we will also discuss briefly self-consistent results obtained with the correlation functional omitted from the potential and several values of the somewhat artificial scale factor α for $V_{ex}(\vec{r})$ (e.g., $\alpha = 0.72$,[23] and the Slater value $\alpha = 1$, currently used in band theory).

We start with an initial guess for the charge density in a form of a *population-dependent* superposition density

$$\rho^{sup}(\vec{r},\{f^{\alpha}_{n,l}, Q^{\alpha}\}) = \sum_{m,l} \rho_{\alpha}(\vec{r} - \vec{R}_m - \vec{d}_{\alpha}, \{f^{\alpha}_{n,l}, Q^{\alpha}\}) \ , \quad (2)$$

where $f^{\alpha}_{n,l}$ and Q^{α} denote the atomic (ionic) orbital population for Ti and S in a central-field (n,l) notation and the net ionic charge of site α, respectively, and $\vec{R}_m$ and $\vec{d}_{\alpha}$ denote lattice vectors and the αth site position vectors, respectively. $\rho_{\alpha}(r,\{f^{\alpha}_{n,l}, Q^{\alpha}\})$ is taken as the self-consistent (spherically symmetric) charge density of atom (ion)α, obtained by solving numerically the local-density one-particle equation for this site. The single-site population numbers and charges are used later as free parameters that are iteratively adjusted so as to minimize the different $\Delta\rho(\vec{r})$ between the crystal charge density and the superposition density. With this choice, the initial potential $V^{sup}(\vec{r})$ is a sum of four terms, $V^{sup}_{SRC}(\vec{r})$; $V^{sup}_{LRC}(\vec{r})$; $V^{sup}_{ex}(\vec{r})$, and $V^{sup}_{corr}(\vec{r})$. Here $V^{sup}_{SRC}(\vec{r})$ and $V^{sup}_{LRC}(\vec{r})$ denote the short-range Coulomb and the long-range Coulomb superposition (initial) potentials, respectively. $V^{sup}_{SRC}(\vec{r})$ is obtained as a lattice sum of the individual one-site Coulomb potentials obtained by solving Poisson's equation for $\rho_{\alpha}(r) + (Z_{\alpha} - Q^{\alpha})\delta(r)$, while $V^{sup}_{LRC}(\vec{r})$ is obtained as an Ewald sum[24] of the residual electrostatic point charges Q^{α}. $V^{sup}_{ex}(\vec{r})$ and $V^{sup}_{corr}(\vec{r})$ are obtained by directly applying the exchange and correlation functionals to the superposition density in Eq. (2). Note that in calculating $V^{sup}_{ex}(\vec{r})$ and $V^{sup}_{corr}(\vec{r})$, the potential is *not* linearized with respect to the individual one-site densities $\rho_{\alpha}(r)$, nor is it spherically averaged around each site as is common in KKR and augmented-plane-wave (APW) techniques. Also, all non-muffin-tin parts both in the short-range Coulomb and in the electrostatic point-ion potential are fully retained in $V^{sup}(\vec{r})$. Owing to the low site symmetry in the TiS_2 structure, these contributions are sizable and cannot be neglected (e.g., a $\frac{3}{4}$-Ry non-muffin-tin potential correction is calculated at the Ti-S bond center). The potential $V^{sup}(\vec{r})$ is converged to 10^{-4} a.u. after the lattice sum in Eq. (2) and in $V^{sup}_{SRC}(\vec{r})$ are extended to 27 a.u. and the Ewald summation is performed up to maximum reciprocal and real-space cutoff distances of $G^2_{max} \leq 51$ a.u.$^{-2}$ and $R_{max} \leq 23$ a.u., respectively. At this state $V^{sup}(\vec{r})$ is fully defined by specifying the atomic numbers, Z_{Ti} and Z_S, the crystal structure and the assumed populations and ionic charges $\{f^{\alpha}_{n,l}, Q^{\alpha}\}$. We note, however, that owing to the nonlinearity of the exchange and correlation functionals with respect to $\rho_{\alpha}(r)$, the superposition potential $V^{sup}(\vec{r})$ is not describable as a simple lattice sum of one-site terms, and hence the solution of the one local-density equations constitutes a multicenter problem.

The crystal eigenfunctions $\psi_j(\vec{k},\vec{r})$ are expanded in the standard LCAO form as linear combinations of Bloch functions $\Phi_{\mu\alpha}(\vec{k},\vec{r})$ constructed from the basis functions $\chi_\mu^\alpha(r)$ of type μ and site α. These are obtained by solving self-consistently for the isolated Ti^{+Q} and $S^{-Q/2}$ species a local-density one-particle equation similar to that used to generate the one-site densities $\rho_\alpha(r)$, but with an added external potential well[25] that acts to suppress the long tails of the virtual atomic orbitals that might cause linear dependence in the Bloch basis set. The radius of this well is chosen so that all core orbitals will be practically unchanged by its presence. The set $\{\Phi_{\mu\alpha}(\vec{k},\vec{r})\}$ obtained in this way is fully defined by the assumed population and charges $\{f_{n,l}^\alpha, Q^\alpha\}$, the crystal structure, and the atomic numbers; a real-space cutoff distance of 21 a.u. is required for 10-ppm accuracy. We use an extended numerical basis set of 1*s*, 2*s*, 2*p*, 3*s*, 3*p*, 3*d*, 4*s*, and 4*p* for Ti, and 1*s*, 2*s*, 2*p*, 3*s*, 3*p*, and 3*d* for S (a total of 46 basis functions).

We next write the linear LCAO equations in the usual way, with the Hamiltonian and overlap matrix elements given in the Bloch basis. These matrix elements are calculated directly by a three-dimensional Diophantine numerical integration scheme.[14-16] (About 5000 integration points were required to obtain an accuracy of 1–3 mRy in the valence and the lowest 9 conduction bands and ~18-mRy accuracy in the core bands.) All the multicenter integrations encountered in conventional LCAO theory are completely avoided, and any general form of the crystal potential or basis set can be treated equally in a straightforward manner.

The secular equation is solved for a set of wave vectors $\{\vec{k}_q\}$ in the irreducible section of the Brillouin zone (BZ) (see notation in Fig. 1) and the resulting wave functions $\{\psi_j(\vec{k}_q,\vec{r})\}$ for all occupied bands are used to compute the crystal density, but with the BZ integration replaced by a discrete summation over the set $\{\vec{k}_p=\Gamma, M, K, A, L, H\}$ with their associated nearest-volume weights. It is found that although the BZ dispersion of the *band* charge density is substantial, the wave-vector-dependent *total* ground-state charge density

$$\rho(\vec{k},\vec{r})=\sum_j n_j(\vec{k})\rho_j(\vec{k},\vec{r})$$

had a much lower dispersion. To evaluate the error introduced by sampling $\rho(\vec{k}_q,\vec{r})$ at a limited $\vec{k}_q$ set, we have calculated its Fourier transform (x-ray scattering factor) across the BZ (Fig. 2). The horizontal lines on the right-hand side of the figure represent the results obtained from the superposition model [Eq. (2)] with the electronic configurations Ti $3d^24s^2$ and S $3s^23p^4$, while the horizontal

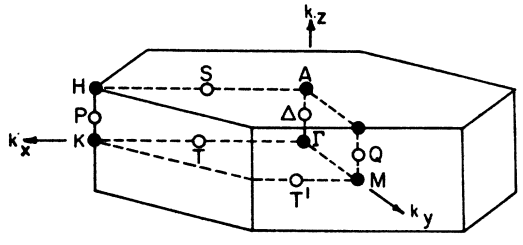

FIG. 1. Brillouin zone (BZ) for the 1*T*-TiS_2 structure.

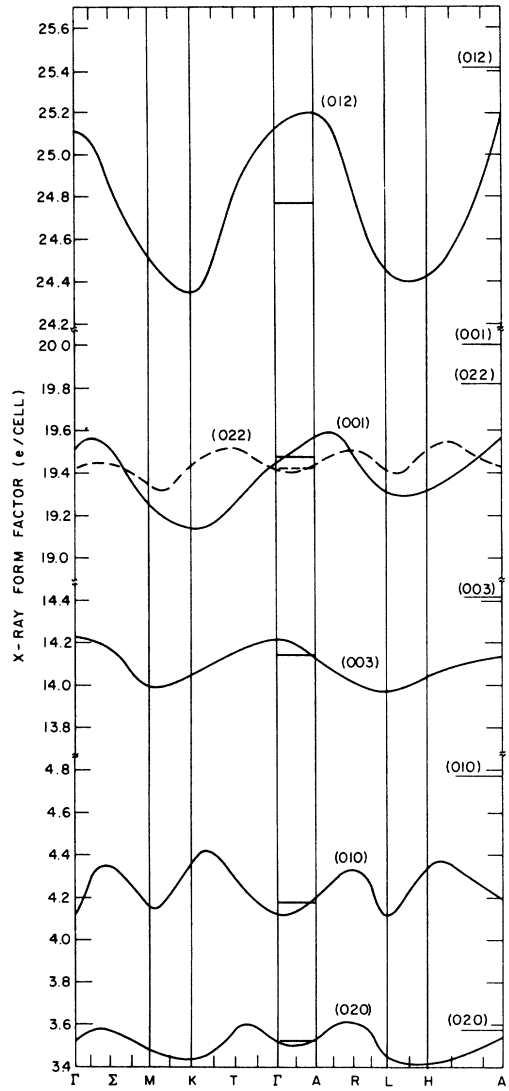

FIG. 2. Dispersion of the $\vec{k}$-dependent scattering factors in TiS_2. The horizontal lines on the right-hand side represent the corresponding structure factors obtained from the initial superposition density [Eq. (2)] using configuration Ti $(3d^24s^2)$ and *S* $(3s^23p^4)$. The horizontal lines between the Γ and *A* points represent the BZ averages. The data were calculated at the 20 $\vec{k}$ values denoted by vertical lines on the abscissa.

lines along the Γ-A line are the BZ averages of the (hkl) scattering factors. It is seen that the maximum dispersion in the six lowest scattering factors does not exceed (1–3)% from their mean value. The largest error in the scattering factors associated with sampling only the 6 $\vec{k}$ values is 0.8% while an 11-point sampling ($\Gamma, \Sigma, M, K, T, A, R, L, S, S', H$) produces a maximum error of 0.5%. We have performed a single calculation of the band eigenvalues at Γ using the charge density sampled at 11 $\vec{k}$ points; the resulting shift in eigenvalues is 5 mRy of which only a 2 mRy shift was nonuniform (i.e., band dependent). Hence, we use the 6 $\vec{k}$ points as a standard sampling set in our calculation.

We note from Fig. 2 that the scattering factors deduced from the superposition model using the configurations Ti $3d^2 4s^2 4p^0$ and S $3s^2 3p^4 3d^0$ are in marked disagreement with those obtained from the crystal wave functions listed in Table I. Clearly, one needs to optimize the input charge density to approach self-consistency.

Self-consistency is obtained in our scheme in two stages; in stage 1 we perform "charge and configuration self-consistency" (CCSC) and in stage 2 a "full self-consistency" (FSC) is obtained. We define CCSC as a consistent relation between the crystal potential and charge density in which the latter is restricted to be representable as a lattice sum of one-center terms located on existing atomic sites. The vast majority of self-consistent treatments in solid-state and molecular theory belong to this class, the main differences between them being the approximation used in choosing the single-site projection set [e.g., a spherical muffin-tin set in the multiple-scattering $X\alpha$ (MS-$X\alpha$) technique,[17] a Slater or Gaussian set in local exchange LCAO molecular studies,[18] etc.]. One realizes that such a procedure of arbitrarily dividing the multicenter charge density $\rho_{\rm cry}(\vec{r})$ into sums of one-center densities centered on a limited number of sites would not produce, in a general case, a reliable representation, leading in many cases to a highly structured and non-negligible residual density[14,26,27]

$$\Delta\rho(\vec{r}) \equiv \rho_{\rm cry}(\vec{r}) - \rho^{\rm sup}(\vec{r}) \ .$$

[This term is treated exactly in our second stage of self-consistency (FSC).]

In our CCSC we vary iteratively the atomic (ionic) orbital population and charges $\{f^{\alpha}_{n,l}, Q^{\alpha}\}$ used to construct both the superposition potential and basis function (by repeating the solution of the *atomic* one-particle equation for a different $\{f^{\alpha}_{n,l}, Q^{\alpha}\}$ set) so as to minimize in the least-squares sense the deviation $\Delta\rho(\vec{r})$ over the unit-cell space. This procedure selects the "best" superposition model in the configuration space defined by the exact numerical one-site orbitals used here, and offers a direct means of varying our orbital basis set *nonlinearly* by allowing them to relax to the current form of the crystal potential. In this procedure, charge is redistributed among the various basis orbitals resulting in hybridization, shift of nodes, and promotion of charge into the formerly virtual orbitals (e.g., Ti $4p$ or S $3d$).

Since any variation in the core population [Ti($1s$, $2s$, $2p$, $3s$, $3p$) and S($1s$, $2s$, $2p$)] had little effect on $|\Delta\rho(\vec{r})|$, and the sulphur $3d$ population changed by less than 2% during iterations, the only remaining effective degrees of freedom were the $\mathrm{Ti}^{+Q_1}(3d^{2-x}4s^{2-y}4p^z)$ and $\mathrm{S}^{-Q_2}(3s^2 3p^{4+Q_2})$ populations where $Q_2 = \frac{1}{2}(x-y-z)$ and $Q_1 = -2Q_2$. A free variation of these parameters yielded (6 iterations were required) a configuration in which $x = 0.02e$, $y = 0.80e$, and $z = 0.40e$ with a Ti net charge of $+0.42e$ and a sulphur charge of $-0.21e$. The standard deviation associated with $\Delta\rho(\vec{r})$ was lowered thereby by a factor of 5.5 relative to the initial neutral $x = y = z = Q_1 = Q_2 = 0$ configuration. The difference between this final charge density and the initial superposition model density with $x = y = z = 0$ is displayed in Fig. 3 along the Ti-S bond direction. It is evident that in the final CCSC stage substantial charge is displaced from the core regions to the interstitial regions with a higher amount of electronic charge attracted to the sulphur site than to the titanium site (indicating a partial ionic character). It is, however, clear from Fig. 3 that even the convergence limit of the CCSC step [in which the basis set was nonlinearly varied and the full nonspherical terms in $\rho^{\rm sup}(\vec{r})$ were retained], the final charge density still deviates (a standard deviation of 0.53 electron/cell) from the true crystal charge $\rho_{\rm cry}(\vec{r})$ obtained from the wave functions. Clearly, in transition-metal compounds like TiS_2 with a highly anisotropic structure and considerable interpenetration of the central-site wave func-

TABLE I. X-ray scattering factors of TiS_2 calculated in the self-consistent exchange and correlation model, in units of electron/atom.

hkl	Scattering factor
(0 0 0)	18.00
(0 1 1)	12.03
($\bar{1}$ 1 3)	3.10
(0 1 2)	8.25
($\bar{1}$ 1 2)	7.82
(0 0 1)	6.57
(0 2 2)	6.41
(0 0 3)	4.70
(0 1 0)	1.65
(0 2 0)	1.23

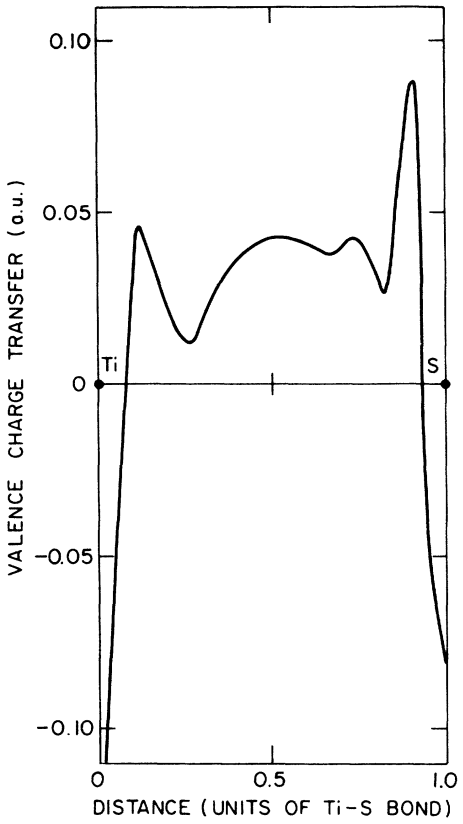

FIG. 3. Difference in valence charge density between the final CCSC result and the initial superposition model density [with the configurations Ti ($3d^2 4s^2$) and S ($3s^2 3p^4$)] along the Ti-S bond direction.

tions into neighboring sites, even a self-consistent superposition scheme is insufficient to describe the full charge anisotropy.

In our final stage in self-consistency (FSC), we take advantage of the fact that in performing stage 1 to convergence all the localized "sharp" features in $\Delta\rho(\vec{r})$ [defined now as charge-density difference between $\rho_{\text{cry}}(\vec{r})$ and the *final* CCSC $\rho^{\text{sup}}(\vec{r})$] are absorbed into the nonlinearly varied $\rho^{\text{sup}}(\vec{r})$ so as to produce a reasonably smooth residual $\Delta\rho(\vec{r})$ with a zero net charge. We hence proceed to FSC by Fourier transforming $\Delta\rho(\vec{r})$ (using a three-dimensional Diophantine integration) for a list of reciprocal-lattice vectors $\vec{K}_s$ and obtain the correction to the Coulomb electronic potential $\Delta V_C(\vec{r})$ due to the residual density $\Delta\rho(\vec{r})$ by analytically solving the associated Poisson equation. The sum over the reciprocal-lattice vectors converges rapidly (only the first seven stars are needed). Next we add $\Delta V_C(\vec{r})$ to $V^{\text{sup}}_{\text{SR}C}(\vec{r}) + V^{\text{sup}}_{\text{LR}C}(\vec{r})$ obtained in the last step of the CCSC and to the refined exchange and correlation potentials calculated directly from $\rho_{\text{cry}}(\vec{r})$. The solution of the eigenvalue problem is now repeated iteratively with this refined Hamiltonian (and the fixed basis set obtained in the last CCSC iteration) so as to diminish the residual density $\Delta\rho(\vec{r})$ obtained in successive iterations. The iterations are terminated when $|\Delta\rho(\vec{K}_s)|$ is smaller than $0.01e$ (four damped iterations were required).

III. BAND-STRUCTURE RESULTS

TiS_2 crystallizes in the trigonal CdI_2 structure (space group $P\bar{3}m$ or D^3_{3d}) with one formula unit per cell and a hexagonal Bravais lattice.[28-31] This phase (also labeled as $1T$ or the C-6 structure) contains two-dimensional planes of S-Ti-S units separated from each other by a "Van der Waals" gap. The Ti atoms are sandwiched between planes of S where the stacks are arranged so that each Ti site lies above another Ti site in the following stack. The S atoms are arranged in a near octahedral sixfold coordination around the Ti site within each sandwich; however, due to a slight trigonal distortion along the c axis, the S-S distances are not identical. The Ti-S distance is 2.4279 Å while the Ti-Ti distance is 3.40 Å. A recent crystallographic determination of the room-temperature lattice parameters of stoichiometric TiS_2 showed the values $a = 3.4073 + 0.0002$ Å and $c = 5.6953 + 0.0002$ Å ($c/a = 1.671$, compared with the ideal $1T$-octahedral value of $c/a = 1.633$) while smaller values were obtained in the older crystallographic work of Benard and Jeannin[30] performed on a nonstoichiometric sample ($a = 3.4048$ Å, $c = 5.6904$ Å). The primitive lattice vectors in this structure are $\hat{l}_1 = \frac{1}{2}a(\sqrt{3}\,\hat{i} - \hat{j})$, $\hat{l}_2 = a\hat{j}$, and $\hat{l}_3 = c\hat{k}$. The atomic positions in the unit cell are given by Ti(0, 0, 0), $S_{(1)}(1/2\sqrt{3}a, \frac{1}{2}a, Zc)$, and $S_{(2)}(1/\sqrt{3}a, 0, -Zc)$, where the parameter Z governing the interlayer separation is not determined by symmetry. Its ideal octahedral value of $\frac{1}{4}$ is close to the observed value.[28]

We assume a perfect crystal arrangement and the best-known lattice parameters,[28] and, using the method outlined in Sec. II, obtain the self-consistent band structure of TiS_2 in the exchange and correlation model shown in Fig. 4. We also denote in this figure the Madellung point-ion corrected free-ion eigenvalues of Ti^{+Q} and $S^{-Q/2}$ (where $Q = 0.42e$, the final CCSC value). It is clear that the energy bands group themselves into several distinct sets. The upper six bands in the valence region (denoted here as VB1 or the bonding "σ" bands) are bonding combinations of sulphur $3p$ and titanium $3d$, $4s$, and $4p$ orbitals. The maximum in the valence band occurs at the Γ_2^- point. Owing to the presence of interlayer bonding, it is not possible to distinguish between σ and π character in the entire BZ; however, at Γ and A the bands are separable into two

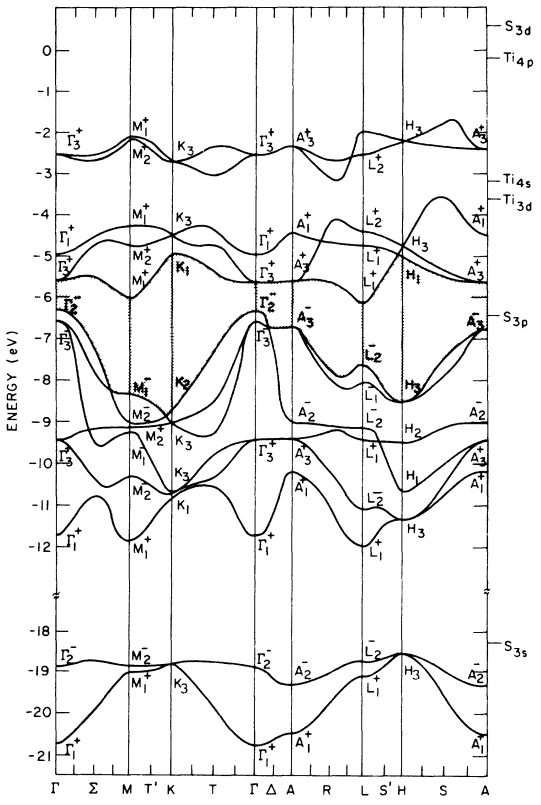

FIG. 4. Self-consistent exchange and correlation band structure of TiS_2. The horizontal lines on the right-hand side denote the free-ion eigenvalues (corrected for the point-ion field in the crystal). The actual calculated points are denoted by the vertical bars on the abscissa. The symbols VB1 and VB2 denote the two lowest groups of valence bands while CB1 and CB2 denote the two lowest d-based conduction bands.

π pairs ($\Gamma_2^- - A_2^-$ and $\Gamma_1^+ - A_1^+$) made up of sulphur $3p_z$ and titanium $4p_z$ and $3d_{z^2}$ orbitals and two σ pairs ($\Gamma_3^+ - A_3^+$) and ($\Gamma_3^- - A_3^-$) made up of the in-plane x-y combination of Ti $3d$, $4s$, $4p$, and S $3p$. The π valence bands show a pronounced dispersion (~2.5 eV) along the Γ-A interlayer direction characterizing a strong interlayer overlap, while the more localized σ orbitals have a much smaller interlayer interaction. Below the VB1 we find a second group of two valence bands (VB2) separated from VB1 by a 6.8-eV gap. These bands have a predominant sulphur $3s$ character and, surprisingly, a non-negligible dispersion (indicating the degree of its non-core-like character). The splitting between the centers of gravity of VB1 and VB2 is 10.3 eV, which is close to the atomic $3s$-$3p$ splitting in sulphur (10 eV). Liang and Cundy,[32] in setting up a phenomenological model for the electron-energy-loss spectra in transition-metal dichalogenides, suggested that the VB2 bands bend upwards towards the VB1 group of bands at the BZ edges so as to form a structure that is similar to that of homonuclear graphite. No such effects are observed in our calculated band structure. We note that the VB1 – VB2 splitting is largely an atomic effect and that due to the heteropolarity of the system, (cf., similar results[33] in hexagonal BN, which is the heteropolar analog of graphite) the low-lying sulphur "$3s$" band cannot overlap with the mixed s-p VB1 band. Below VB2 we have the Ti $3p$ band at −39.1 eV, the Ti $3s$ band at −61.7 eV, the S $2p$ at −15.6 eV, and the S $2s$ band at −209.5 eV, etc. These bands (not shown in Fig. 4) are very narrow and atomiclike in character; however, their center of gravity deviates in position from the point-ion corrected free-ion eigenvalues by as much as 1–3 eV due to the substantial core-shifts introduced by the overlapping tails of the neighboring wave functions. Similarly, the position of the nodes in their corresponding wave functions are shifted by as much as 0.5 a.u. relative to the free-ion limit due to a substantial valence-electron screening in the solid. Thus, a simple frozen core treatment of these states seems to be inappropriate.

The antibonding σ^* counterpart of the bonding VB1 bands is located between +1.0 eV to about +10 eV above vacuum (not shown in Fig. 4) and has a predominantly Ti $4s$, $4p$, and S $3d$ character with some S $3s$, $3p$ contributions. In this large σ-σ^* gap are located the two d-like conduction bands (denoted here as CB1 and CB2, respectively). These bands are formed from Ti $3d$ orbitals with a sizable contribution from Ti $4p$, $4s$, and S $3p$, $3d$. The lower band (CB1, denoted loosely in crystal-field terminology as the "t_{2g}" band) is about 2.5 eV wide, while the higher one (CB2 or "e_g" band) is 1 eV wide with a center-of-gravity crystal-field gap of 2.3 eV separating it from CB1. Owing to the trigonal distortion from the ideal octahedral symmetry, CB1 is split into a twofold representation (Γ_3^+ and A_3^+) and a singly degenerate representation (Γ_1^+ and A_1^+) with about a 0.5-eV $\Gamma_3^+ - A_1^+$ gap. The minimum in CB1 occurs at the L_1^+ point with a second local minimum at M_1^+. The indirect valence-to-conduction gaps are 0.23 eV at $\Gamma_2^- - L_1^+$ and 0.29 eV at $\Gamma_2^- - M_1^+$ with a larger direct gap of 0.84 eV at Γ. The calculated direct gaps at M and L are 2.5 and 1.6 eV, respectively.

The band structure along the Γ-M-K direction deviates from that along the parallel A-L-H directions due to interlayer interactions. These deviations are pronounced in the valence bands while they are much smaller in the CB1 and CB2 bands due to the negligible participation of the Ti $3d$ orbitals in interlayer bonding. Similarly, the large σ-σ^* bonding-antibonding gap is indicative of ad-

vanced $s-p$ bonding in the system.

While our band structure is qualitatively similar to previously published results,[6-8,34,35] it is clear from the above that some fundamental differences occur. Here we note that the order of bands obtained in this work is at variance with that obtained previously [e.g., the position of the valence Γ_3^--Γ_2^- and M_1^--M_2^- pairs is interchanged with the KKR results[6] and the position of the conduction levels Γ_1^+-Γ_3^+ and A_1^+-A_3^+ pairs is interchanged with the orthogonalized-plane-wave (OPW) results[34]]. Further, the empirical LCAO work of Murray and Yoffe,[7,8] with parameters adjusted to reproduce the three lowest optical transitions, yields a very small conduction-band width (2.04 eV), split by only 1.5 eV, and a similar underestimation in the VB1 width (2.8 eV). Similarly, the KKR work[6] predicts a too narrow d-based bandwidth (2.7 eV) with a narrow gap of only 1.2 eV between CB1 and CB2.

Recently, a self-consistent OPW calculation on TiS_2 was published by Krusius *et al.*[34] This work indicates a VB1 width of 6.6 eV with a 5.5-eV gap between this band and the VB2 (width 2.5 eV). While these characteristics of the valence band agree with our results, the nature of the conduction bands differ considerably; the OPW indicates very large direct gaps at Γ, M, and L (3.7, 3.7, and 3.4 eV, respectively, compared with our results of 0.8, 2.5, and 1.6 eV, respectively) with a very small (0.2 eV) CB1–CB2 splitting. We also note that their calculated gaps *increase* (by about 0.8 eV) when the exchange coefficient α is increased between $\frac{2}{3}$ and 1, while our calculations, as well as the KKR[6] and the molecular[35] calculations, clearly indicate a pronounced *decrease* of energy gaps with increasing α. Further, the calculated OPW transition energies disagree with experiment and show very considerable qualitative differences in the order of the conduction levels as obtained in this work. Similar pathologies in OPW calculations of d bands in transition-metal compounds (lacking a d core) have been previously[36] attributed to a lack of sufficient plane-wave convergence. We suspect that similar problems in the work of Krusius *et al.*[34] might be responsible for the substantial differences they obtain with the present results and with the experimental data.

IV. COMPARISON WITH EXPERIMENT

A. Optical properties

The optical properties of TiS_2 in the visible and ultraviolet were investigated by reflectance,[3] transmission,[37,38] and electron-energy-loss[32,39] experiments shown in Fig. 5. In all cases, the spectrum starts with a steep free-carrier line at

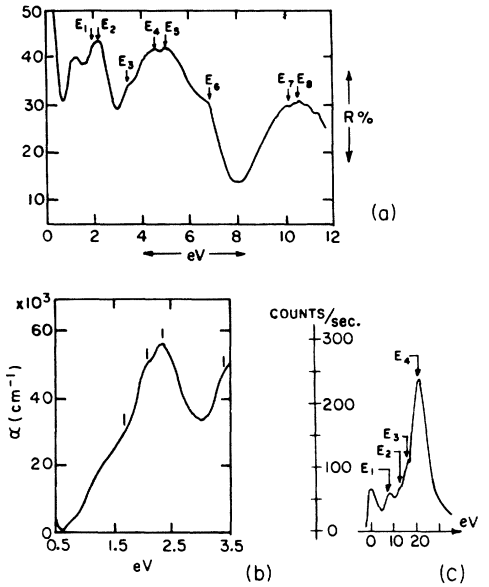

FIG. 5. Observed (a) reflectance (Ref. 3); (b) transmission (Ref. 37); and (c) electron energy loss (Ref. 39) of TiS_2.

0–0.5 eV, that is probably due to excess Ti atoms in the nonstoichiometric samples. The absorption coefficient μ starts with the characteristic $\mu^{2.0}(E)$ dependence.[38] The overall spectra in the 0–20-eV region for the electric vector $\vec{E}$ perpendicular to the crystal c axis can be separated into three regions with large dips in the absorption coefficient ("windows") between them (Fig. 5): the first region extending up to 2.8 eV followed by a window at ~3.0 eV (region I), then a broad region up to the second window at ~8 eV (region II), and finally the region extending to 20 eV (region III). Two plasmon bands appear at 7.4 and 22.3 eV corresponding to the collective excitations of 4 and 16 electrons, respectively.[39] Unlike the more ionic members of the layered dichalcogenides group (e.g., CdI_2), no excitons have been clearly identified in the spectra of TiS_2; it would thus seem that all the structure observed in regions I–III originates from interband transitions. We will account for these transition energies in our theoretical model.

Since TiS_2 has an easy cleavage plane parallel to the layer direction, all optical experiments were done for an $\vec{E}\perp\vec{c}$ polarization of the electric vector $\vec{E}$. Hence, we listed in Table II the calculated transition energies between all high-symmetry points that are connected by an allowed $\vec{E}\perp\vec{c}$ transition (some selection rules are given in Refs. 8 and 40), and collect the closely spaced transitions into single groups. These results are compared with the experimental transmission,[36,37] reflectance,[3] and electron-energy-loss[39] spectra. The

TABLE II. Experimental and calculated transition energies at high-symmetry points in the BZ of TiS_2 for the $\vec{E} \perp \vec{c}$ polarization. Values are given in eV.

Transition	Calc.	Expt.	Transition	Calc.	Expt.
1. $\Gamma_3^- \rightarrow \Gamma_3^+$	1.02	1.04,[a] 1.22,[b] 1.03[c]	7. $L_2^- \rightarrow L_2^+$	5.03	5.0[b]
$\Gamma_2^- \rightarrow \Gamma_3^+$	0.84				
2. $\Gamma_3^- \rightarrow \Gamma_1^+$	1.65	1.64,[a] 1.4[c]	8. $\Gamma_3^- \rightarrow \Gamma_1^+$	6.81	6.80[b]
$L_2^- \rightarrow L_1^+$	1.63		$K_2 \rightarrow K_3$	6.55	
			$M_2^- \rightarrow M_2^+$	6.76	
3. $L_1^- \rightarrow L_1^+$	2.04	2.01,[a] 1.95[b]	9. $\Gamma_3^- \rightarrow \Gamma_1^+$	10.0	10.1[b]
			$A_3^- \rightarrow A_1^-$	10.2	
4. $L_2^- \rightarrow L_1^+$	2.36	2.29,[a] 2.20,[b] 2.1[c]	10. $M_1^- \rightarrow M_2^-$	10.7	10.5[b]
$M_1^- \rightarrow M_1^+$	2.54		$L_2^- \rightarrow L_1^+$	10.8	
5. $\Gamma_3^- \rightarrow \Gamma_3^+$	3.96	3.37,[a] 3.35,[b] 3.2[c]	11. $H_3 \rightarrow H_2$	11.2	11.0[b]
$L_2^- \rightarrow L_2^+$	3.22				
$\Gamma_2^- \rightarrow \Gamma_3^+$	3.80				
6. $K_3 \rightarrow K_2$	4.50	4.50[b]	12. $\Gamma_2^- \rightarrow \Gamma_3^+$	13.3	13.6[d]
$K_2 \rightarrow K_3$	4.55		$M_2^- \rightarrow M_2^+$	13.6	
			$L_2^- \rightarrow L_1^+$	13.2	
			13. $\Gamma_1^+ \rightarrow \Gamma_3^+$	15.8	16.0[d]
			$L_2^- \rightarrow L_1^+$	16.1	

[a] Transmission, $T = -268\,^{\circ}C$ (Ref. 37).
[b] Reflectance, $T = 20\,^{\circ}C$ (Ref. 3).
[c] Transmission, $T = 625\,^{\circ}C$ (Ref. 38).
[d] Electron energy loss (Ref. 39).

agreement with experimental results is seen to be very good. The spectra is divided into three regions; the transitions labeled 1–5 in Table II occur between levels in VB1 and the lower d-based conduction-band CB1 levels. These transitions are separated by a 2.3 eV window from the second group which consists of VB1– CB2 type transitions and extending from about 4 to 7 eV (transitions 6–8 in Table II). The second window separating the VB1-CB transitions from VB1-σ^* (antibonding) transitions occurs at 7–10 eV and is followed by the σ-σ^* absorption region above 10 eV (transitions 9–11 in Table II). The lower S 3s-based valence bands (VB2) are excited to the d-based conduction bands CB1 and CB2 at around 13 eV. These optical transitions in the region above 13 eV might overlap the high-energy tail of the σ-σ^* transitions. Finally, the collective excitation of all (16) VB1 + VB2 electrons appears as a plasmon peak at around 19–22 eV.[39] Although only a detailed calculation of the imaginary part of the dielectric constant would enable a definite assignment of the transitions, the general excitation pattern observed here appears to be correct.

Our assignment in the low-energy region parallels that of Murray and Yoffe in their empirical LCAO calculation,[7] but disagrees with the previous KKR assignment based on a 1.4-eV shift in the calculated excitation energies.[6] The origin of the first and second transmission windows agrees qualitatively with the assignment of Fischer[41] based on a molecular-orbitals model (and the data of Sonntag *et al.*[42]) although a more detailed comparison with his simplified molecular energy-level scheme is not possible. We also note that the diffuse leading absorption edge observed in the 0–0.5-eV region,[3,37,38] previously suggested to arise from an indirect gap,[7,8] corresponds to our minimum $\Gamma_2^- - L_1^+$ and $\Gamma_2^- - M_1^+$ gaps (0.23 and 0.29 eV, respectively) or alternatively to free-carrier absorption. A non-negligible temperature dependence of the transmission peak at 2.29 eV might be indicative of an exciton transition,[37] although further experimental work would be needed to verify its existence.

The lowest direct interband transition[3,37,38] at 1.03–1.22 eV was previously observed to shift to lower energies with increased Ti content in the sample.[38] It was argued that this provides evidence for a CB1-σ^* type transition and rules out a VB1-CB1 transition since the energy of the latter would increase with increasing Ti content due to additional population of CB1 by the excess Ti 3d electrons. We note here that the conduction-band minima occur at M and L (and not at Γ) and only these states are expected to be populated by a slight excess of Ti 3d electrons (and hence shift to higher energies) while the transition at 1.03–1.22 eV assigned here to a Γ_3^+ final state (being some 0.6 eV higher than M_1^+ and L_1^+) is actually found to shift to lower energies with increased Ti 3d population,[43] in agreement with experiment.[42]

TABLE III. Calculated and experimental values for the band-structure features in TiS_2. Values are given in eV.

	Expt.	Calc.
Width of VB1	6–7, [a] 4.0–4.5, [b] 6–7 [c]	5.5
VB1-VB2 gap	6–7, [b] 7–8 [d]	6.8
Width of VB2	2–3, [a] 1–2 [b]	1.9
Total CB width	4[10]	3.6
CB1-CB2 splitting	2.1, [c] 2.2 [d]	2.3

[a] He photoemission (Ref. 10).
[b] X-ray photoemission (Ref. 11).
[c] Appearance potential spectra (Ref. 12).
[d] X-ray absorption (Ref. 41).

The general pattern and splittings in the valence bands of TiS_2 were investigated by x-ray photoemission[10,11] and absorption,[42] while similar information on the lowest conduction bands was obtained in appearance potential spectra.[12] The results of these studies, summarized in Table III (together with our calculated results), reveal a broad valence-band split into two components: the first (VB1), extending from the Fermi level to about −6 eV[41] with a mean width[9,10] of 6–7 eV (versus a width of only 4.0–4.5 eV observed in photoemission[11]), is separated by a gap of about 6–7 eV from the lowest valence-band group (VB2), which has a width of about 2–3 eV with its center of gravity at 13 eV below the Fermi level.[41] The x-ray absorption spectra[42] in the sulphur L_{II} and L_{III} region and in the titanium $M_{III,II}$ region exhibit a separation of 2.3 eV between transitions to the two lowest unoccupied bands. These were identified with the two lowest Ti $3d$-based conduction bands (CB1 and CB2, respectively). This splitting is consistent with the observed width of the first window in the optical spectra of TiS_2,[3] and with a similar splitting observed in x-ray emission.[41] The $L_{III,II}$ appearance-potential spectrum of Ti in TiS_2 shows a broad conduction band[42] (width ~4 eV) that is split into two distinct components with a gap of 2.1 eV between them, in good agreement with the x-ray absorption and emission data for the CB1-CB2 splitting. The agreement between the observed and the calculated valence- and conduction-band width and splittings is very good.

The weak photoemission peak observed[7–9] at 0–0.5 eV below the Fermi energy does not appear in our calculated band structure. This structure was previously attributed to a small overlap between VB1 and the lowest edge of the d-based CB1 band, in agreement with the observed semimetallic electrical conductivity of TiS_2.[2,3] Our calculation predicts a 0.2–0.3-eV gap between VB1 and CB1 and this appears to rule out such a mechanism in the perfect crystal. Note, however, that the photoemission studies were performed on relatively imperfect crystals so that the nature of the observed photoemission peak (intrinsic VB1-CB1 overlap, the presence of some disorder induced states,[9] impurities, or excess Ti electrons due to nonstoichiometry[7,8]) could not be determined. The He II photoemission data[7,8] are consistent with the presence of some 0.05 electrons/Ti atom (which might also be denoted by impurities) while the x-ray data of Wertheim *et al.*[9] and Fischer[34] is consistent with an interpretation of a degenerate semiconductor with a gap smaller than 0.2–0.5 eV (in contradiction with the prediction of all other calculations[4–6,34]). The orbital character of the electrons responsible for the low-energy photoemission peak still awaits further experimental investigation (e.g., electron-spin resonance or nuclear-quadrupole resonance).

The reflectance of TiS_2 in the infrared (ir) region has been studied by Lucovsky *et al.*[44,45] Out of the nine vibrational modes in the Brillouin-zone center, only one (E_u) is ir active (with polarization $\vec{E} \perp \vec{c}$). The ir reflectance in the 0–4000-cm^{-1} region reveals a broad and structureless plasmon mode with no evidence for a lattice vibrational mode. Fitting the reflectance spectra with a single plasmon mode dielectric formula resulted in a very large high-frequency dielectric constant ($\epsilon_\infty = 13.7$[44]) and a plasma frequency of 6900 cm^{-1} (0.86 eV). This would lead to a high effective transverse charge e_T^* of about $5.9e$[44], in contrast to the much lower e_T^* values (~$0.5e$) for the group-VI metal dichalcogenides. If dynamic charge redistribution effects taking place during the vibrational excitation are neglected, this high e_T^* value for TiS_2 would imply a highly ionic bonding with a formal valency of about +4 for Ti, in the static limit. Lucovsky *et al.*[44,45] found that this extreme ionic structure is inconsistent with the observed interatomic distances in the crystal [(i.e., the sum of the tabulated Ti and S (S-S) ionic radii is larger than the observed mean Ti-S (S-S) distance in the crystal] and concluded that the bonding in the solid is predominantly metallic with a large dynamic contribution to the effective charge. They supported this conclusion by the observation that the Ti electronic configuration ($3d^2 4s^2 4p^0$) is far from the d^2sp^3 configuration required for covalent bonding in octahedral symmetry. However, as discussed in Sec. V, our calculated valence wave functions indicate substantial covalent bonding together with a high ($4.6e$) effective charge. We also find that the promotion energy between a $3d^2 4s^2 4p^0$ electronic configuration to a $3d^2 4s^1 4p^1$ configuration (having an open-shell sp hybrid orbital avail-

able for bonding in the crystal) is rather small (1.5–2.0 eV) and easily compensated by the covalent bond energy and the additional electrostatic field formed by the Madellung crystal-field potential.

B. Transport properties

The transport properties of TiS_2 have recently received considerable attention. Thompson[5] reported a T^2 dependence of the electrical resistivity in TiS_2 in the range $T = 10–400$ °K. On the basis of the analysis of the Seebeck coefficient, Hall effect, and resistivity data[29] it is concluded that the resistivity can be factored into a rigid-band temperature-independent effective-mass term and a relaxation time term which contains all the temperature dependence and is dominated by electron-electron scattering. The magnitude of the observed resistivity as well as its $n^{-5/3}$ dependence on the free-carrier concentration n was consistent with an electron-hole scattering mechanism. The nature of this scattering mechanism (i.e., electron-electron, electron-hole, etc.) is a subject of great interest and discussion.[46,47]

The most likely origin of the observed transport properties of TiS_2, based on the small indirect gap found from our self-consistent calculations, lies in the presence of a small amount of impurities even in the stoichiometric samples. This seems consistent with the absence of de Haas–van Alphen signals in even the best samples.[48]

We suggest here an additional mechanism which can contribute to the explanation of the observed conductivity in the presence of an apparent small band gap. The experimental Seebeck coefficient versus the changes in the susceptibility on doping TiS_2 with excess titanium[4] indicates a very large spectroscopic splitting factor $g = 4.3$. Such a large value, which is required to explain the positive magnetic susceptibility in this material, was also observed in other semimetals when the band gap approaches the value of the spin-orbit splitting in the system.[49] The soft-x-ray spectrum[42] of TiS_2 suggests a Ti $3p$ spin-orbit splitting of 1.3 eV which is substantially higher than the estimated *atomic* value of 0.7 eV.[50] The atomic Ti $3d$ and S $3p$ spin-orbit splittings are 0.06 and 0.09 eV, respectively; however, an enhancement factor such as that implied by observed Ti $3p$ splitting would bring the calculated gap in TiS_2 quite close to the spin-orbit splitting and hence would explain the large g value observed in this material. Such a situation can favor a semimetallic behavior due to electron-hole scattering arising from hole pockets at Γ in the valence band and electrons in the L (and M) conduction-band minima. Although crude, we feel such a model can help to illuminate the ambiguity between the transport data and the band model. Detailed relativistic calculations are needed to assess the validity of this hypothesis.

V. CHARGE DENSITY AND BONDING IN TiS_2

A. Charge analyses, wave functions, and bonding mechanisms

The bonding mechanism in transition-metal compounds in general,[17,51–54] and TiS_2, in particular,[35,44,45] have been the subject of a substantial number of controversial studies. The role of metallic d bonding versus a covalent s,p bond as well as the degree of ionicity in this structure is not properly understood at this time. In an attempt to clarify this situation we undertook a detailed study of the wave functions and charge density in TiS_2.

We start with the question: "How much of the atomiclike titanium $3d$, $4s$, $4p$, and sulphur $3s$ and $3p$ character are present in the ground state of TiS_2 crystal?" First we note two features of this general problem: (i) There is always a considerable degree of arbitrariness in attempting to partition the multicenter crystalline charge density into partial waves associated with individual sites. In principle, there exists a large number of ways of doing this (e.g., projecting the crystalline charge into an arbitrary muffin-tin representation and expanding the spherical charge in partial waves,[52] performing a Mulliken charge analysis, etc.); each way, however, leads to a distinctly different answer. Hence, we consider here the partitioning of the crystal charge density only as a rough guide for the electronic structure of the solid, and in doing so we will avoid any additional approximation to the density itself (e.g., muffin tin). (ii) The orbital population in the solid indicates the degree to which each one-site spherical wave is variationally *mixed* in the ground state, but does not tell us anything about its contribution to *bonding* (i.e., to form an enhanced wave-function overlap and thus to increase the cohesive energy). With these remarks in mind, we chose three partitioning schemes for the crystal charge density: (a) the Mulliken population analysis[55] in which the orbital charge is identified with the square of the corresponding basis-set coefficient plus one half of the orbital bond charge; (b) the Löwdin population analysis[56] in which the Bloch basis is first orthogonalized (using an $S^{1/2}C$ transformation where S is the overlap matrix and C is the coefficient matrix) and the orbital charge is then identified with the square of the transformed coefficients in the nonoverlapping basis; and (c) the minimum-deviation CCSC electronic configuration, i.e., the orbital population that minimizes in the least-squares sense the deviation between the cry-

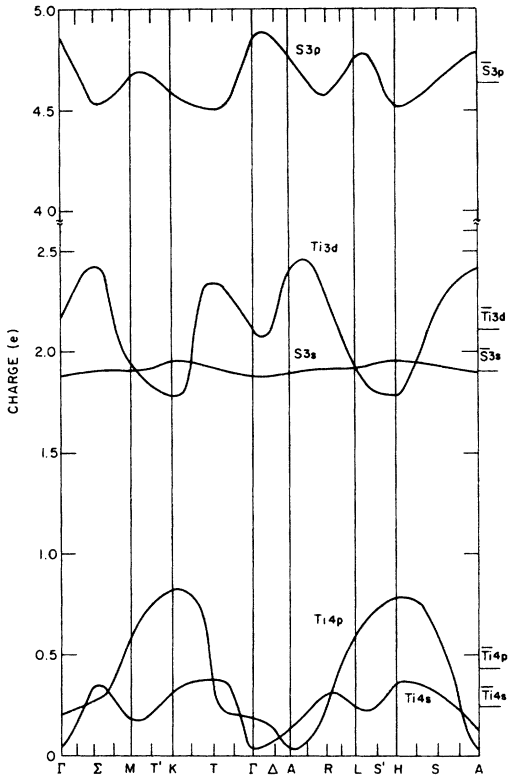

FIG. 6. BZ dispersion of the Mulliken orbital charge in TiS_2. The horizontal lines on the right-hand side denote the corresponding BZ averages.

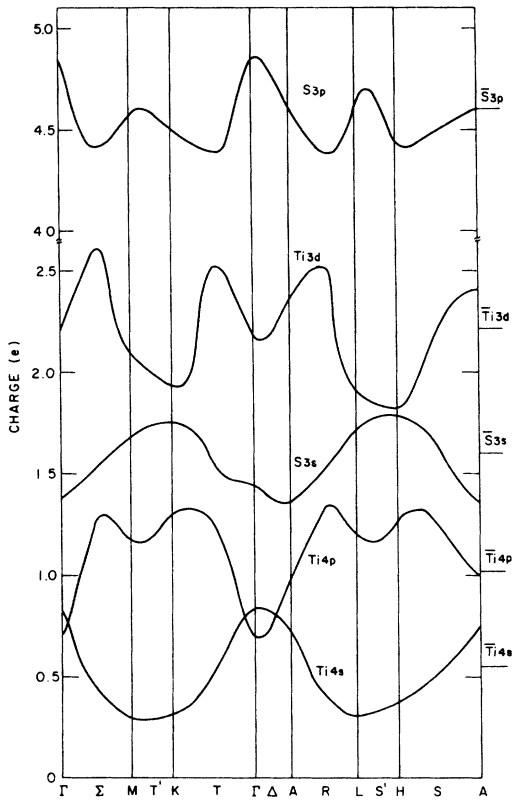

FIG. 7. BZ dispersion of the Löwdin orbital charge in TiS_2. The horizontal lines on the right-hand side denote the corresponding BZ averages.

stal and the superposition charge density.

Figures 6 and 7 show the Mulliken and Löwdin orbital charges, respectively, along high-symmetry directions in the BZ, as calculated from the FSC crystal wave functions of all occupied (core plus valence) bands at 21 $\vec{k}$ points in the irreducible zone. The corresponding BZ averages are indicated by the horizontal bars on the right-hand side. The results of these population analyses are only qualitatively similar: the orbital character along the Γ-M-K lines resembles that of the A-L-H lines; the Ti $3d$ population reaches a minimum near K and H and has several maxima near Σ, T, and R, etc. Note the large difference in the dispersion of the S $3s$ population and the generally larger dispersion obtained in the Löwdin versus the Mulliken analyses. Both calculations show a considerable depletion of the Ti $4s$ orbital (populations of $0.25e$ and $0.55e$ in the Mulliken and Löwdin schemes, respectively) along with a substantial charge promotion into the formerly unoccupied Ti $4p$ orbital (final populations of $0.44e$ and $1.02e$ in the Mulliken and Löwdin schemes, respectively). The sulphur $3s$ population oscillates slightly below its free-atom value while the S $3p$ population shows a 0.4–$0.6e$ increase over the free-atom value. The quantitative differences between the Mulliken and Löwdin populations are easily apparent. In the Löwdin scheme the orbital charges are "softer," showing more pronounced dispersion than in Mulliken's scheme, and a lower charge polarization. The BZ-averaged Mulliken is $Ti^{+1.19}$ $(3d^{2.12}4s^{0.25}4p^{0.44})$ and $S^{-0.595}$ $(3s^{1.91}3p^{4.435}3d^{0.25})$, and the final Löwdin population is $Ti^{+0.22}$ $(3d^{2.21}4s^{0.55}4p^{1.02})$ and $S^{-0.11}$ $(3s^{1.62}3p^{4.40}3d^{0.09})$. These configurations should be contrasted with the converged CCSC result of $Ti^{+0.42}$ $(3d^{1.98}4s^{1.20}4p^{0.40})$ and $S^{-0.21}$ $(3s^{1.92}3p^{4.20}3d^{0.09})$. We note that the results obtained by different partitioning schemes differ considerably, and that none of them correspond to any physically significant charge.

The following general conclusions, however, appear to be valid: (i) The important *intra-atomic* charge rearrangements taking place in forming the crystal from atoms are the titanium $4s$ to $4p$ charge promotion and the sulphur $3s$ to $3p$ promotion, with the Ti $3d$ orbital population remaining very close to its ground-state atomic value of two. (ii) The leading *interatomic* charge redistribution involves transferring of titanium $4s$ charge to the

sulphur $3p$ orbitals, resulting in a net $Ti^{+Q}S_2^{-Q/2}$ configuration. Note that the valence VB1 and VB2 bands alone contain enough Ti $3d$ character to account for the Ti $3d^2$ structure without population of the $3d$-based CB1 and CB2 bands, and that the calculated p/s hybridization ratio of sulphur in its crystalline bonding state (2.4–2.7) is rather close to the ideal sp^3 structure required for octahedral bonding, contrary to previous suggestions.[54] Our results indicating a substantial Ti $4p$ population in the ground state are in agreement with the sizable Ti $4p \rightarrow 1s$ emission band (observed in the x-ray band spectra[11]) and in disagreement with the assumptions made in previous band studies on TiS_2.[7,8] In a calculation in which Ti $4p$ character was absent in the assumed variational basis set, we found that more Ti $4s$ charge was shifted to the sulphur orbitals (owing to the difficulty of providing extensive Ti $3d-4s$ intra-atomic charge transfer) resulting in higher ionicity of the structure and enhanced band gaps (σ-σ^* and VB1-CB1). This point seems to have been overlooked in previous LCAO studies of transition-metal compounds which indicate large band gaps and relatively narrow bands.[7,8] On the other hand, we observe that the sulphur $3d$ states play a relatively minor role in the occupied states in TiS_2 affecting only a small reduction in the ionicity of the structure.

As stated previously, the point charges calculated from the charge density by any of the partitioning schemes discussed above does not tell us about the contribution of particular orbitals to bonding, nor does it indicate whether the calculated formal ionic charge corresponds to an actual charge transfer between the atoms in the unit cell or just to wave-function overlap. To clarify these points one has to examine the crystalline wave functions. Some self-consistent valence-band wave functions along the Ti-S bond direction for several high-symmetry $\vec{k}$ points are given in Fig. 8, omitting for clarity any orbital coefficient that contributes less than 5%. We see that while the Ti $3d$ orbital [Fig. 3(a)] hardly forms any enhanced charge build up in the bond region, the Ti $4s$ orbitals, and to some extent the Ti $4p$ [cf., Figs. 8(c) and 8(b)], act to produce a strong bonding combination. We also note that while the Ti $4s$ and $4p$ orbitals penetrate deeply into the sulphur core region so as to shift the S $3p$ node away from the atomic origin [Figs. 8(b) and 8(c)], the Ti $3d$ orbitals are too localized for that purpose, and, as a matter of fact, they are just slightly changed in shape relative to the free-atom limit (volume effects being taken into account). Hence, we conclude that although Ti $3d$ character is *mixed* quite considerably into that occupied manifold, our variational calculation indicates little *bonding* occurs with these orbitals. We

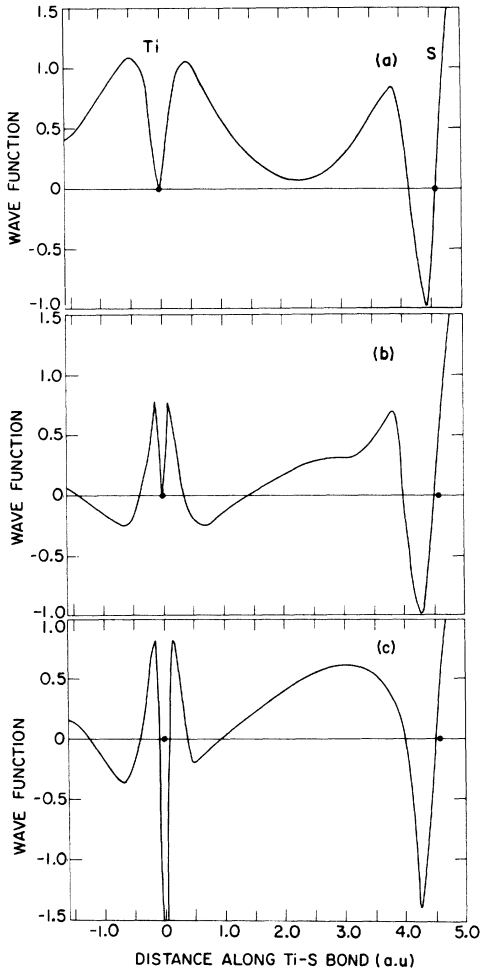

FIG. 8. Wave function of the occupied bands in TiS_2 along the Ti-S bond. (a) Ti $3d$ S $3p$ state at M_2^+; (b) Ti $4p$ S $3p$ state at M_1^-; (c) Ti $4s$ S $3p$ state at K_1. The black dots on the abscissa indicate the positions of the atoms.

further note that the very-long-range character of the Ti $4s$ and $4p$ orbitals results in a considerable overlap of these functions on the sulphur sites, but that an actual ionictype charge transfer cannot be implied (this is consistent with the fact that the ionicity of the atomic species that yield the best CCSC result is indeed very small). Thus, these results do not agree with previous suggestions of metal $3d$ bonding to the nonmetal atoms in transition-metal clusters,[47,54] and with similar ideas put forward to Lucovsky *et al.*[44] in interpreting the ir effective transverse charge of TiS_2.

Another point worthy of investigation arises from the high optical transverse charge e_T^* of TiS_2. Infrared measurements[44,45] seem to dictate a e_T^* value of about $5.9e$ which is about 6–7 times larger than that observed for group-VI dichalcogenides

(e.g., MoS_2). In the absence of dynamic effects (i.e., change of effective charge due to the vibrational displacement) a highly ionic $Ti^{4+}S_2^{2-}$ structure would be predicted, as is indeed assumed by Chianelli *et al.*[28] in their attempt to fit the observed structure factors in TiS_2 by an atomic model. To investigate this point, the effective charge was calculated directly from the self-consistent charge density. We start by computing the molecular unit-cell dipole along the Ti-S direction λ by integrating $\vec{r}_\lambda \rho(\vec{r})$. To minimize the contribution of the surface polarization (due to net charge transfer across the cell boundary[57]) to the total polarization, the integration is confined to a volume enclosed by a minimum equipotential contour ($V = 0.02$ a.u.) marking the molecular boundaries inside the cell. Direct Diophantine numerical integration yields an electronic moment of $1.4ea_0$ (which is consistent with a rather low point charge of $+0.4e$ on Ti and $-0.2e$ on S). We then compute the dipole moment using the same lattice constants as before but with an A_{1g}-type symmetrical distortion (with amplitude of 0.001 a.u.) on the atomic position. The necessary displacement derivative of the dipole moment[58] is then simply calculated by taking the numerical derivative. This procedure yields an effective charge e_T^* of $4.6e$ which is considerably larger than the calculated static point charge ($0.42e$) implied from the nonvibrating dipole and agrees reasonably well with the experimental estimate. Clearly, TiS_2 has a very low static ionicity which differs distinctly from its large dynamic ionicity associated with the highly polarizable $4s$ and $4p$ orbitals (the change in dipole moment associated with these orbitals contributes 62% to the dynamic charge).

B. Energetics of bonding

We concentrate here on the relation between the assumed electronic population of Ti and S in the atomic limit and the energetics of bonding the crystal. It has been a common practice in APW- and KKR-type calculations for transition-metal compounds[6,59] to use a crystalline potential field derived from a superposition of atomic potentials in their *ground state* [viz., $Ti(3d^24s^2)$ and $S(3s^23p^4)$]. Since many studies of the band structure of transition metals have indicated changes in the eigenvalues by as much as a factor of 2–3 upon modifying the atomic population numbers, these were used as "free" parameters adjusted so as to obtain agreement with experiment for some measured quantities.[60] Here we study the effect of the assumed populations from a variational point of view, examining their effect on the *total energy* of the system. We have previously described our methods for obtaining the total crystal energy in the numerical LCAO approach[14,15] and have demonstrated that good accuracy can be obtained for the absolute total energy in solids made up of first-row atoms (diamond,[61] BN, and LiF[62]). Since we are not able to present to obtain a similar level of accuracy in the absolute total energy of transition-metal compounds (because the presence of a large number of core electrons necessitates very high accuracy in integrating the associated oscillatory core density, and its very large contribution to the total energy), the cohesive energy cannot be reliably computed. However, the *relative* total energies (between band calculations with different assumed atomic configurations) can be computed to an accuracy of about 0.3 eV using 8000 Diophantine integration points if the two corresponding band calculations do not differ in the core contributions to the density. This accuracy is sufficient for our present purpose.

To investigate the electronic population effects on bonding in TiS_2 we have chosen three configurations for titanium: (I) $3d^{2+Q}4s^{2-Q}4p^0$, (II) $3d^24s^{2-Q}4p^Q$, and (III) $3d^24s^14p^Q$. In the first configuration the $4s$ population is depleted in favor of the $3d$ population, while in the second configuration the $4s$ population is depleted in favor of the $4p$ population. Both these configurations leave the titanium atom neutral and are hence associated in the crystal with a neutral configuration for sulphur of the type $S(3s^23p^4)$. In configuration (III) we allow for ionic character on the Ti (for $Q < 1$) and associate this configuration with a charged sulphur atom $(3s^23p^{4+(1-Q)/2})$.

The observed[63] ground state of the Ti atom is due to configuration (I) with $Q = 0$ (which is degenerate with configuration II with the same Q), and gives rise to a series of multiplets (^3F, ^1G, ^3P, ^1D) with an energy spread of about 0.15 eV. The next state in energy is due to configuration I with $Q = 1$; its associate multiplet band starts at about 0.8 eV above the ground state. At higher energies one finds configuration II with $Q = 1$ which lies some 1.9 eV above the ground state. Analytic (Slater) Hartree-Fock atomic calculations[64] give the $3d^34s^1$ state at only 0.54 eV above the ground state while a Gaussian basis calculation[65] shows that the average of energies of the lowest triplets arising from the $3d^24s^14p^1$ configuration lies slightly *lower* than the $3d^34s^1$ configuration average. Since the width of both the valence band and the d-based conduction band in TiS_2 is much larger than these energy differences, it seems that both configurations (I + II) have to be considered. Configuration III was also included since it is degenerate with configuration II at $Q = 1$ and allows for ionic character at lower Q.

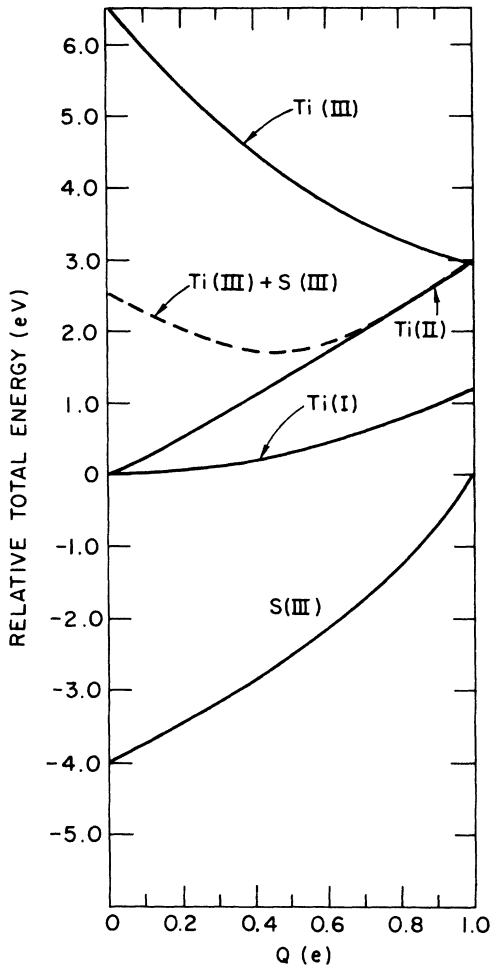

FIG. 9. Atomic total energies for Ti and S as a function of electronic configuration in the local-density approximation. The zero level is chosen as the $3d^2 4s^2$ and $3s^2 3p^4$ ground-state configurations for Ti and S, respectively. The titanium configurations are: (I) $3d^{2+Q} 4s^{2-Q} 4p^Q$; (II) $3d^2 4s^{2-Q} 4p^Q$; (III) $3d^2 4s^1 4p^Q$ while the sulphur configuration is $3s^2 3p^4$ for (I) and (II) and $3s^2 3p^{4+(1-Q)/2}$ for configuration (III).

Figure 9 shows the *atomic* total energies calculated in the local-density approximation as a continuous function of populations (variation of Q) for the different channels in configurations I–III. Unlike the case of the compound, atomic total energies can be obtained to high accuracy by use of standard one-dimensional integration techniques. The zero level was set as the Ti $3d^2 4s^2$ and S $3s^2 3p^4$ ground-state configurations for titanium and sulphur, respectively. The results parallel the experimental configuration averages as discussed above. It is seen that when titanium changes its configuration (by changing Q) along channel I, its total energy increases by about 1 eV for $Q = 1$ and leads to an open shell $4s^1$ orbital that is capable of forming an $s-p$ bond in the crystal. A higher promotion energy (~2.8 eV) is required when the atom changes its configuration along channel II, but now both $4s$ and $4p$ orbitals are capable of forming bonds in the solid. In both cases, the sulphur atom remains neutral and thus stays at the same relative total energy (denoted here as the zero reference level). When Ti changes its configuration with decrease of Q from $Q = 1$ along the ionic channel III, its energy increases by as much as 2.8–6.5 eV; here both a $4sp$ hybrid can be formed and a positive charge developed on this site which would cause, in turn, an electrostatic Madellung-type stabilization in the crystal. The sulphur atom in the corresponding ionic $3s^2 3p^{4+(1-Q)/2}$ configuration [marked S(III) in Fig. 9] lowers its total energy along this channel by as much as 4 eV. The dashed curve in Fig. 9 denotes the relative total energy of a structure of one Ti and two S atoms, both changing their configuration along channel III. It is seen that although configuration III seems too high in energy for Ti, the accompanying decrease in the sulphur total energy makes the combined process reasonable in terms of energy cost (only 1.73 eV above the ground state of Ti + 2S atoms compared with a maximum of 2.8 eV for configuration II). Although crude, these simple atomic total energy arguments predict a minimum for configuration III at a titanium net charge of about $0.5e$ which turns out to be not too far from our final self-consistent result for the solid. Thus, in a relatively narrow total energy region of about 1.7 eV, there are three possible classes of titanium configurations which may compete in forming the bonded crystal: the first has $3d$ and $4s$ orbitals available for bonding; the second also has an $4p$ open shell; and the third has, in addition, an associated point-ion electrostatic field. Of course only a variational calculation for the solid can confirm their relative importance.

Figure 10 shows, on a relative energy scale, the total *crystal* energy per unit cell as obtained in separate non-self-consistent calculations with different atomic configurations. For convenience, we have chosen the zero value of relative crystal total energy to coincide with that yielded by the Ti $3d^2 2s^2$ configuration ($Q = 0$ in I and II). In each of these calculations both the superposition crystal potential and the numerical basis set are constructed from the corresponding atomic configuration (cf., Sec. III). We see that the $3d^2 4s^2$ structure has a relatively high total crystal energy (due to the availability of only $3d$ orbitals for effective bonding in the solid). Splitting the closed shell $4s^2$ orbital results in enhanced stabilization (I with $Q \neq 0$) while further $4p$ population (II) produces even stronger binding. Structure III yields the

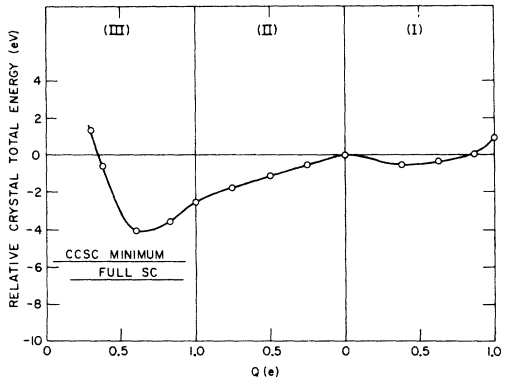

FIG. 10. Relative total crystal energies as calculated from various input atomic configurations. CCSC minimum indicates the relative total energy obtained in the fully optimized CCSC model while the full SC level indicates the total energy on this scale obtained at the full self-consistent limit.

lowest total energy with a minimum at $3d^2 4s^1 4p^{0.6}$ (corresponding to $Ti^{0.4+}S_2^{0.2-}$) and a stabilization of about 4 eV per unit cell over the $3d^2 4s^2$ structure. These results agree with the predictions of the simple atomic model discussed above.

One realizes, of course, that the structures I–III do not span the entire configuration space available for the Ti and S atoms. Indeed, a fully optimized CCSC treatment yields a slightly different configuration (as discussed in Sec. II) and a lower total energy (denoted by a horizontal line at −5.8 eV). As expected, a full self-consistent treatment (in which the individual atomic configurations lose their meaning) results in an even higher-energy stabilization (also indicated by the horizontal lines in Fig. 10). However, our basic conclusions that the stability of the TiS_2 crystal stems from Ti $4sp$ to S $3sp$ ionic-covalent bonding with little participation of Ti $3d$ seems nevertheless valid in view of the relatively small total energy changes introduced by full self-consistency.

It is instructive to consider the various energy band gaps obtained in the non-self-consistent calculations for TiS_2 with the various assumed atomic configurations (Fig. 11). We see that configuration I yields very high gaps at M and L in accordance with the predictions of the atomic model, with the direct Γ-Γ^* gap decreasing with increasing $3d$ population. Calculation of the Mulliken and Löwdin populations for this structure shows that the $3d$ orbital always contains significantly less charge than the prescribed $2+Q$ population, indicating a substantial departure from self-consistency. On allowing $4p$ population, the band gaps decrease, and the charge analysis of the occupied bands indicates a stabilization of the $3d$ population around $2e$ together with a depletion of $4s$ population

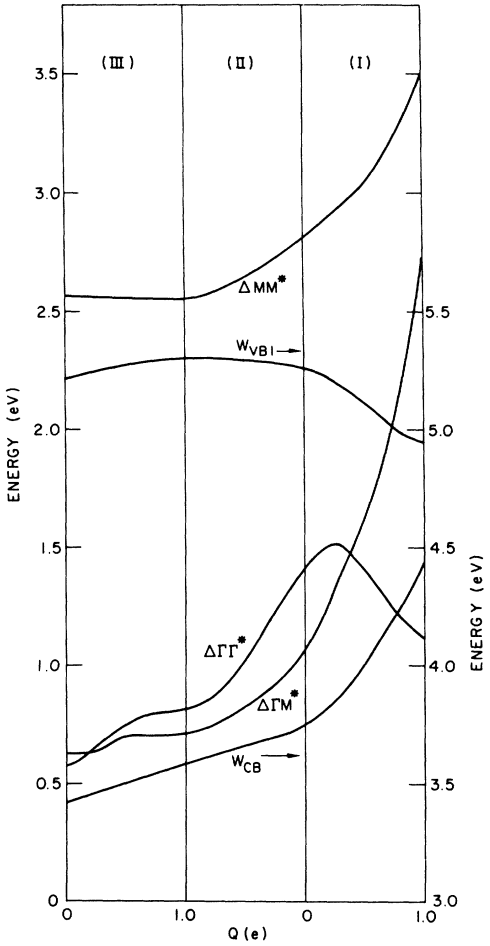

FIG. 11. Changes in the major band gaps and widths with assumed atomic configurations. $\Delta\Gamma\Gamma^*$, ΔMM^*, and $\Delta\Gamma M^*$ indicate the lowest Γ-Γ, M-M, and Γ-M bands gaps, respectively. W_{CB} and W_{VB1} indicate the total width of the d-based conduction band and first valence band, respectively.

in favor of $4p$ and sulphur $3p$. This is consistent with the lowering in energy of the atomic $4s$ level relative to the $3d$ level in going from I to II and III. The stabilized $4s$ and $4p$ levels can now participate more effectively in bonding. We find that the amplitude of the Ti $4s$ charge density at the sulphur nucleus in the solid increases from $0.55e$/a.u.^{3} for the $3d^2 4s^2$ configuration to $1.64e$/a.u.^{3} for the optimal configuration III case, indicating effective wave-function penetration in the latter case. The substantial changes in the calculated gaps and bandwidth observed in Fig. 11 emphasize the weakness of non-self-consistent calculations with their *ad hoc* assumptions of atomic configurations.[59] Further, the results obtained in Fig. 10 stress the importance of using a variational rather than an empirical criterion for choosing the atomic configuration for a band calculation.

TABLE IV. Comparison of non-self-consistent results for the band structure using differing basis sets, an exchange coefficient $\alpha = 1$, and the old lattice constants (Ref. 30). Values are given in eV.

Quantity	Slater set (Ref. 35)	Minimal numerical set	Extended numerical set
Width of VB1	4.25	4.54	4.56
Width of VB2	1.03	1.36	1.36
VB1-VB2 gap	9.88	7.77	7.76
$\Gamma\Gamma^*$ gap	1.91	1.32	1.01
MM^* gap	2.29	2.60	2.32
LL^* gap	2.32	1.98	1.77
ΓM^* gap	1.71	0.92	0.84
ΓL^* gap	1.67	0.83	0.73
Ti 3s band	−74.76	−68.2	−68.1
Ti 3p band	−51.62	−44.9	−44.8
S 2p band	−183.67	−170.8	−170.8

VI. DISCUSSION OF EFFECT OF VARIOUS COMPUTATIONAL PARAMETERS ON RESULTS OBTAINED

We have indicated in the foregoing that the absence of self-consistency is a major reason for both the qualitative and quantitative differences in the results of previous calculations with those of the present model. Here we will briefly discuss the effects of further approximations used in band models for transition-metal compounds. Since previous non-SC calculations on TiS_2 were carried out using the old lattice constants,[30] an exchange coefficient of one, and with the correlation functional omitted, we repeated our calculation under the same conditions so as to facilitate the comparison.

In Table IV we examine basis-set effects on the calculated band structure. We show the results obtained by Ellis and Seth[35] using an analytic (Slater-type) atomic Hartree-Fock basis set (this calculation was extended by us to include also $\vec{k}$ points other than Γ) together with our results for a minimal numerical (i.e., no virtual orbitals) and for an extended numerical basis set. It is seen that a numerical basis set has a significant effect on the valence-to-conduction band gaps while the valence band is reasonably described by the analytic set. This difference probably stems both from the inconsistency of using a Hartree-Fock basis set with a local exchange crystal potential and from the absence of nonlinear variation in the analytic set (our calculation indicates a contraction of about 30% in the optimized 4s orbital relative to the free-atom value). We also give in Table IV energy values for some of the core bands; the corresponding values in the free atom are 66.9, 43.8, and 170.7 eV for Ti, 3s, Ti 3p, and S 2p, respectively. The extended numerical set is seen to reduce somewhat the calculated gaps, but has little effect on both core and valence bands. Experimentation with different extended sets resulted in only small differences from the results shown here.

We next compare the results of our LCAO model with those of the muffin-tin KKR model[6] in the non-self-consistent limit. Both calculations presented in Table V use the same exchange coefficient lattice constant and assume identical atomic configurations for the potential construction. We use our best extended numerical set so as to minimize the differences with the well-converged KKR set. The remaining difference is in the potential employed; the muffin-tin approximation was made in the KKR model, whereas the full potential was used in the LCAO model. The results presented in Table V indicate consistency in the description of the valence band together with substantial differences [(20–90)%] in the width and position of the d-based conduction band, relative to the valence band. The APW calculations of Mattheiss[59] on similar compounds indicated that non-muffin-tin corrections in the intersphere region are responsible for some 20% increase in the d-band width and a 10% reduction in the Γ-Γ^* band gap. He also showed that these intersphere corrections lower the individual band edges by as much as 40%, and enhance the metal-chalcogen bond by lowering the potential barrier between the atoms. Although this explanation is consistent with our discussion of the bond formation, we find the order of magnitude of the calculated intersphere muffin-tin corrections too small to explain the discrepancies found here. It is thus possible that the nonspherical corrections inside the inscribed spheres (these are quite sizable and anisotropic

TABLE V. Comparison of the non-self-consistent KKR and extended LCAO basis calculations for $\alpha = 1$. The lattice constants in both cases are taken from Ref. 30 and an identical atomic configuration of Ti ($3d^2 4s^2$) S ($3s^2 3p^4$) is used. Values are given in eV.

Quantity	MT-KKR (Ref. 6)	LCAO
Width of VB1	5.11	4.56
Width of CB1	1.51	1.93
Width of CB2	1.03	1.38
Total CB width	2.73	3.45
CB1-CB2	1.2	2.3
Γ-Γ^* gap	2.0	1.01
M-M^* gap	2.82	2.32
L-L^* gap	2.27	1.77
Γ-M^* gap	1.44	0.84
Γ-L^* gap	1.40	0.73
VB1 maximum	Γ_3^-	Γ_2^-
CB1 maximum	L_1^+	L_1^+

TABLE VI. Comparison between various self-consistent models with different treatment of exchange and correlation. α_{VT} indicates the mean of Schwarz's (Ref. 23) values for Ti and S (= 0.72). Values are given in eV.

Quantity	Exchange model $\alpha = \frac{2}{3}$	Exchange and correlation model	Exchange model α_{VT}	Exchange model $\alpha = 1$
Width of VB1	5.64	5.49	5.45	4.56
Width of VB2	1.97	1.94	1.67	2.23
VB1-VB2 gap	6.77	6.76	7.67	7.75
Width of CB	3.64	3 59	3.83	2.98
Γ-Γ^* gap	0.87	0.84	0.78	0.098
M-M^* gap	2.60	2.51	2.51	2.36
L-L^* gap	1.65	1.63	1.60	1.31
Γ-M^* gap	0.32	0.29	0.27	0.01
Γ-L^* gap	0.27	0.23	0.23	0.00

in the LCAO model due to substantial core penetration from neighboring sites) might be responsible for the remaining differences (this anisotropy of charge and potential close to the atomic sites is spherically averaged in both APW and KKR models).

We finally examine the effects of exchange scaling and the correlation potential on the band structure (Table VI). We performed fully self-consistent calculations for the points Γ, L, and M using exchange models with $\alpha = \frac{2}{3}$, 0.72, and 1.0.

The results indicate that upon increasing α the major band gaps decrease drastically and that for *$\alpha = 1$ the gaps at L and M vanish*. This behavior under exchange scaling stems from the different sensitivity of VB1 and CB1 wave functions to the exchange: while the upper valence bands (VB1) are characterized by wave functions which are rather delocalized and spread on both the Ti and S sublattices, the wave functions at L and M in the conduction-band edge are much more localized (mostly on the Ti sublattice) and hence stabilize to a larger extent by increasing the exchange potential. We do not think, however, that the choice $\alpha = 1$ is physically meaningful and prefer the use of the Kohn and Sham exchange (with $\alpha = \frac{2}{3}$) and correlation potential. Columns 1 and 2 in Table VI show the results obtained in the pure exchange model with $\alpha = \frac{2}{3}$, and those obtained in a separate exchange and correlation calculation (using the correlation potential of Ref. 20). It is seen that the correlation functional acts to decrease the band gaps and bandwidth (hence making the results more similar to those obtained with $\alpha_{VT} = 0.72$), but that the overall change is rather small.

VII. SUMMARY AND CONCLUSIONS

A fully self-consistent numerical-basis-set LCAO calculation was performed on TiS_2 in the local-density model. The calculated optical transition energies in the 0–16-eV range as well as the various width, gaps, and splittings compare very favorably with optical electron energy loss, photoemission, x-ray absorption, and appearance potential spectra. We find significant differences with previous non-self-consistent muffin-tin calculations as well as with the OPW calculation of Krusins *et al.*[34]

In particular we note the following conclusions:

(i) An indirect gap at M and L of 0.2–0.3 eV persists in the structure. We estimate the possible error in this calculated gap due to computational approximations (e.g., number of Diophantine integration points, BZ summation points, basis-set size, and cutoff distance in direct space summations) to be around 0.10–0.15 eV. We find the gap to be only slightly reduced (at the self-consistent limit) by either increasing the exchange coefficient α from $\frac{2}{3}$ to the virial value (0.72) or by introducing the (nongradient) correlation functional, while only a much larger α value ($\lesssim 1$) produces a vanishing gap. It is stressed, however, that such a value of α is not considered realistic in the context of the local-density model. We note that a nonlocality in the potential (such as that introduced by higher-order correlation terms) will act differently on the band edges at the Γ and L points, and thus might affect the value of the indirect gap. The semimetallic enhancement in the observed g value is tentatively explained by a near coincidence between the energy gap and the enhanced spin-orbit splitting, in agreement with the soft-x-ray data on TiS_2 and with similar effects observed in other semimetals. The small value of the calculated band gap is in contradiction with previous calculations and results from the self-consistent screening of the d-based bands by the

4*s* and 4*p* states as well as by the interatomic charge transfer from Ti to S.

(ii) The bonding in TiS_2 is predominantly covalent and based on overlap of Ti 4*sp* oribitals with S 3*p* orbitals; the Ti 3*d* wave functions play a relatively insignificant role in bonding, although they are appreciably mixed into the occupied bands. No metallic bonding is found in TiS_2, in contradiction with previous suggestions.

(iii) The TiS_2 structure is characterized by a low static ionicity but large dynamic ionic effects due to the polarizability of the diffuse Ti 4*sp* wave functions. The large formal charges obtained from population analysis of the wave functions do not imply actual charge transfer but result instead from wave-function overlap.

Finally, we may use our results for TiS_2 to make some informed speculations about the band structure of $TiSe_2$ and its properties. The earlier KKR calculations[6] for $TiSe_2$ gave a direct band gap of 1.2 eV and an indirect gap of ~0.5 eV (vs 2.0 and 1.4 eV for TiS_2). Extrapolating these trends in the case of our self-consistent calculations indicates that the indirect band gap in $TiSe_2$ is *negative*, i.e., the conduction band at L (and M) is lower in energy than the valence band at Γ (and possibly at A), and gives rise to its semimetallic behavior. Angle-resolved photoemission studies on Ti_xSe_2 (with x somewhat greater than one) show[66] that the conduction band at M dips below the top of the valence band at Γ. (Unfortunately, similar studies of the band states at L have not been reported.) Bachrach *et al.*[66] concluded that stoichiometric $TiSe_2$ would be a semimetal. Recently, DiSalvo *et al.*[67] studied more closely stoichiometric samples and found $TiSe_2$ to be a semimetal with a small band overlap and a low number of carriers.

Recent interest in $TiSe_2$ has centered on the unusual $2a_0$ by $2c_0$ superlattice which forms in $TiSe_2$ at low temperature.[5] Wilson[68] has suggested that this might be an example of the so-called excitionic state[69] rather than a charge-density wave state such as that found in the group-V layered dichalcogenides.[2] Woo *et al.*[70] studied the intensity of x rays diffracted by the superlattice, magnetic susceptibility, resistivity, and far-infrared reflectivity, as a function of temperature in nonstoichiometric samples. Their results showed that the transition observed at $T_0 = 145 \pm 5$ K is second order and they concluded that it was apparently a normal-to-commensurate transition driven by the Fermi surface which has a highly two-dimensional character. Recent neutron studies[67] on stoichiometric samples found $T_0 = 202$ K involving transverse atomic displacement with wave vector $\vec{q} = (\frac{1}{2}, 0, \frac{1}{2})$; this transition was interpreted as being driven by electron-hole coupling.

Our TiS_2 results, extrapolated as above to the case of $TiSe_2$, are consistent with this interpretation. With empty (hole) states at Γ and occupied (electron) states at L (and M), the electron-hole coupling can be strong, particularly if their Fermi surfaces are close to nesting and/or if volume effects (i.e., parallel bands near E_F spanned by the same $\vec{q}$ vector) are important—as appears to be the case for $TiSe_2$. In addition to this electron-hole coupling, the nature of the electron Fermi surface—namely, nearly two dimensional with large nesting between the flat parallel sections of the Fermi surface in planes perpendicular to the z axis in the zone—can give rise to electron-electron (intraband) coupling maxima in the generalized susceptibility $\chi(\vec{q})$ as in the case of $1T$-TaS_2 and $TaSe_2$, and result in possible experimental consequences. Calculations of the electronic band structure of $TiSe_2$ are in progress.

ACKNOWLEDGMENT

The authors thank A. Thompson for stimulating discussions.

†Supported by the NSF (through NU MRC), the Air Force Office of Scientific Research and ERDA.

[1]J. A. Wilson and A. D. Yoffe, Adv. Phys. 18, 193 (1969).
[2]J. A. Wilson, F. J. DiSalvo, and S. Mahajan, Phys. Rev. Lett. 32, 882 (1974); Adv. Phys. 24, 117 (1975).
[3]D. L. Greenaway and R. Nitsche, J. Phys. Chem. Solids 26, 1445 (1965).
[4]A. H. Thompson, H. R. Pisharody, and R. F. Koehler, Phys. Rev. Lett. 29, 163 (1972).
[5]A. H. Thompson, Phys. Rev. Lett. 35, 1786 (1975).
[6]H. W. Myron and A. J. Freeman, Phys. Rev. B 9, 481 (1974).
[7]R. B. Murray and A. D. Yoffe, J. Phys. C 5, 3038 (1972).
[8]R. B. Murray, R. A. Bromley, and A. D. Yoffe, J. Phys. C 5, 746 (1972).
[9]F. R. Shepherd and P. M. Williams, J. Phys. C 7, 4416 (1974).
[10]P. M. Williams and F. R. Shepherd, J. Phys. C 7, L36 (1973).
[11]G. K. Wertheim, F. J. DiSalvo, and D. N. E. Buchman, Solid State Commun. 13, 1225 (1973).
[12]C. Webb and P. M. Williams, Phys. Rev. B 11, 2082 (1975).
[13]R. Huisman, R. De Jonge, C. Haas, and F. Jellinek, J. Solid State Chem. 3, 56 (1971).
[14]A. Zunger and A. J. Freeman, Int. J. Quantum Chem. Symp. 10, 383 (1976).
[15]A. Zunger and A. J. Freeman, Phys. Rev. B (to be published).

[16]D. E. Ellis and G. S. Painter, Phys. Rev. B 2, 2887 (1970).
[17]K. H. Johnson and F. C. Smith, in *Computational Methods in Band Theroy*, edited by P. M. Marcus, J. F. Janak, and A. R. Williams (Plenum, New York, 1971), p. 377.
[18]E. J. Baerends, D. E. Ellis, and P. Ros, Theor. Chim. Acta 27, 339 (1972); H. Sambe and R. H. Felton, J. Chem. Phys. 62, 1122 (1975).
[19]W. Kohn and L. J. Sham, Phys. Rev. A 140, 1133 (1965).
[20]K. S. Singwi, A. Sjölander, P. M. Tosi, and R. H. Land, Phys. Rev. B 1, 1044 (1970).
[21]P. Hogenberg and W. Kohn, Phys. Rev. B 136, 864 (1964).
[22]L. Hedin and B. I. Lundqvist, J. Phys. C 4, 2064 (1971).
[23]K. Schwarz, Phys. Rev. B 5, 2466 (1972); Theor. Chim. Acta 34, 225 (1974).
[24]M. P. Tosi, Solid State Phys. 16, 1 (1964).
[25]R. E. Watson, Phys. Rev. 111, 1108 (1958); F. W. Averill and D. E. Ellis, J. Chem. Phys. 59, 6412 (1973).
[26]R. F. W. Bader and A. D. Bandrank, J. Chem. Phys. 49, 1653 (1968).
[27]A. R. Lubinsky, D. E. Ellis, and G. S. Painter, Phys. Rev. B 11, 1537 (1975).
[28]R. R. Chianelli, J. C. Scanlon, and A. H. Thompson, Mater. Res. Bull. 10, 1379 (1975).
[29]A. H. Thompson, F. R. Gamble, and C. R. Symon, Mater. Res. Bull. 10, 915 (1975).
[30]J. Benard and Y. Jeannin, Adv. Chem. 39, 191 (1963).
[31]H. P. B. Rimmington and A. A. Balchin, J. Cryst. Growth 21, 171 (1974).
[32]W. Y. Liang and S. L. Cundy, Philos. Mag. 19, 1031 (1969).
[33]A. Zunger, A. Katzir, and A. Halperin, Phys. Rev. B 13, 5560 (1976).
[34]P. Krusius, J. Von Boehm, and H. Isomaki, J. Phys. C 8, 3788 (1975).
[35]D. E. Ellis and A. Seth, Int. J. Quantum Chem. Symp. 7, 223 (1975).
[36]R. N. Euwema, D. J. Stuckel, and T. C. Collins, in *Computational Methods in Band Theory*, edited by P. M. Marcus, J. F. Janak, and A. R. Williams (Plenum, New York, 1971), p. 82.
[37]A. R. Beal, J. C. Knights, and W. Y. Liang, J. Phys. C 5, 3531 (1972).
[38]P. B. Perry, Phys. Rev. B 13, 5211 (1976).
[39]M. R. Vilanove, C. R. Acad. Sci. Paris B 271, 1101 (1970).
[40]C. Y. Fong and M. L. Cohen, Phys. Rev. B 5, 3095 (1972).
[41]D. W. Fischer, Phys. Rev. B 8, 3576 (1972).
[42]B. Sonntag and F. C. Brown, Phys. Rev. B 10, 2300 (1974).
[43]This difference in behavior originates from the fact that unlike the M_1^+ and L_1^+ levels, the Γ_3^+ level contains sizable Ti 4*s* contributions that stabilize this level with increased Ti 3*d* contribution. See discussion of population effects in Sec. V B and Fig. 11 for different trends in the ΓM, ΓL vs the $\Gamma\Gamma$ gap with Ti 3*d* population.
[44]G. Lucovsky, R. M. White, J. A. Benda, and J. F. Revelli, Phys. Rev. B 7, 3859 (1973); G. Lucovsky, W. Y. Liang, and R. M. White, Solid State Commun. 19, 303 (1976).
[45]R. M. White and G. Lucovsky, Solid State Commun. 11, 1369 (1972).
[46]A. J. Freeman and A. Zunger, Bull. Am. Phys. Soc. 21, 261 (1976).
[47]C. A. Kukkonen and P. F. Maldague, Phys. Rev. Lett. 37, 782 (1976).
[48]A. J. Freeman, H. W. Myron (Nijmegen, The Netherlands); A. Arko (Argonne National Laboratory) (private communication).
[49]C. Herring, in *Magnetism*, edited by G. T. Rado and H. Suhl (Academic, New York, 1966); also M. H. Cohen and E. I. Blount, Philos. Mag. 5, 115 (1960).
[50]F. Herman and S. Skillman, *Atomic Structure Calculations* (Prentice-Hall, Englewood Cliffs, N.J., 1963).
[51]A. B. Kunz, M. P. Guse, and R. J. Blint, J. Phys. B 8, L358 (1975); R. J. Blint, A. B. Kunz, and M. P. Guse, Chem. Phys. Lett. 36, 191 (1975).
[52]A. Neckel, P. Rastl, R. Eibler, P. Weinberger, and K. Schwarz, J. Phys. C 9, 579 (1976).
[53]J. F. Alward, C. J. Fong, M. El-Batanouny, and F. Wooten, Solid State Commun. 17, 1013 (1975).
[54]R. P. Messmer, S. K. Knudson, K. H. Johnson, J. B. Diamond, and C. Y. Yang, Phys. Rev. B 13, 1396 (1976).
[55]R. S. Mulliken, J. Chem. Phys. 23, 1833 (1955).
[56]P. O. Löwdin, J. Chem. Phys. 18, 365 (1950).
[57]J. D. Jackson, *Classical Electrodynamics* (Wiley, New York, 1961), p. 112.
[58]B. I. Bennett and A. A. Maradudin, Phys. Rev. B 5, 4146 (1972).
[59]L. F. Mattheiss, Phys. Rev. B 8, 3719 (1973).
[60]S. L. Altman and C. J. Bradley, Proc. R. Soc. Lond. 92, 764 (1967).
[61]A. Zunger and A. J. Freeman, Phys. Rev. B 15, 5049 (1977).
[62]A. Zunger and A. J. Freeman (unpublished).
[63]C. E. Moore, Atomic Energy Level Tables, Natl. Bur. Stds. (U.S.) Circ. No. 467 (U.S. GPO, Washington, D.C., 1949), Vol. 76.
[64]E. Clementi and C. Roetti, At. Data Nucl. Data Tables 14, 185 (1974).
[65]S. Topiol, J. W. Moskowitz, C. F. Melius, M. D. Newton, and J. Jafri, ERDA Research and Development Report No. C00-3077-105, New York University (1976) (unpublished).
[66]R. Z. Bachrach, M. Skibowski, and F. C. Brown, Phys. Rev. Lett. 37, 40 (1976).
[67]F. J. Di Salvo, D. E. Moncton, and J. V. Waszczak, Phys. Rev. B 14, 4321 (1976).
[68]J. A. Wilson (private communication).
[69]B. I. Halperin and T. M. Rice, Rev. Mod. Phys. 40, 755 (1968).
[70]K. C. Woo, F. C. Brown, W. L. McMillan, R. J. Miller, M. J. Schaffman, and M. P. Sears, Phys. Rev. B 14, 3242 (1976).

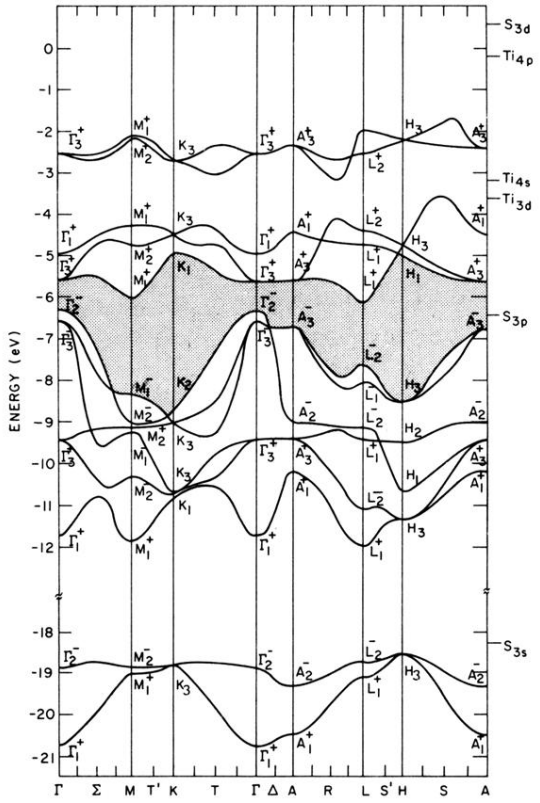

FIG. 4. Self-consistent exchange and correlation band structure of TiS_2. The horizontal lines on the right-hand side denote the free-ion eigenvalues (corrected for the point-ion field in the crystal). The actual calculated points are denoted by the vertical bars on the abscissa. The symbols VB1 and VB2 denote the two lowest groups of valence bands while CB1 and CB2 denote the two lowest d-based conduction bands.